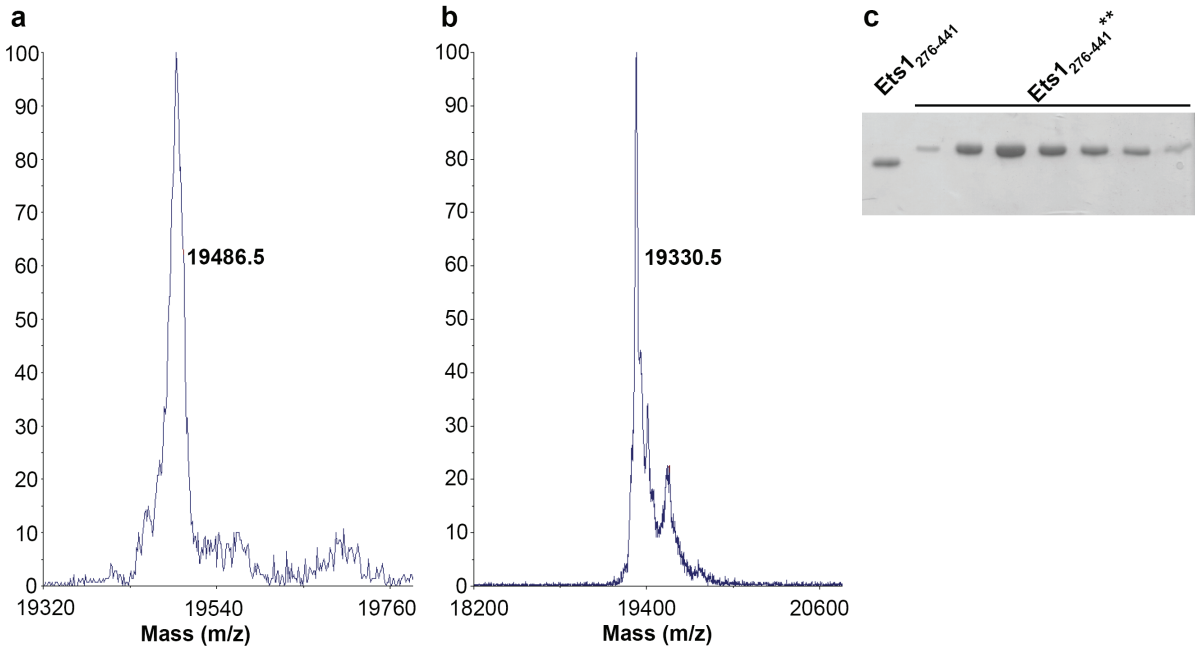

Supplementary Figure 1. Characterization of $Ets1_{276-441}$ phosphorylation. (**a**) and (**b**) MALDI spectra of phosphorylated $Ets1_{276-441}$** and non-phosphorylated $Ets1_{276-441}$. The difference of molecular weights between $Ets1_{276-441}$** and $Ets1_{276-441}$ is 156 Da. This corresponds to two phosphates in $Ets1_{276-441}$** with molecular weight of 80 Da. (**c**) Coomassie blue-stained SDS PAGE of $Ets1_{276-441}$ and $Ets1_{276-441}$**. Lane 1 – purified $Ets1_{276-441}$; lane 2 to 8 – purified fractions $Ets1_{276-441}$** from Mono Q™ 5/50 GL (GE Healthcare) column.

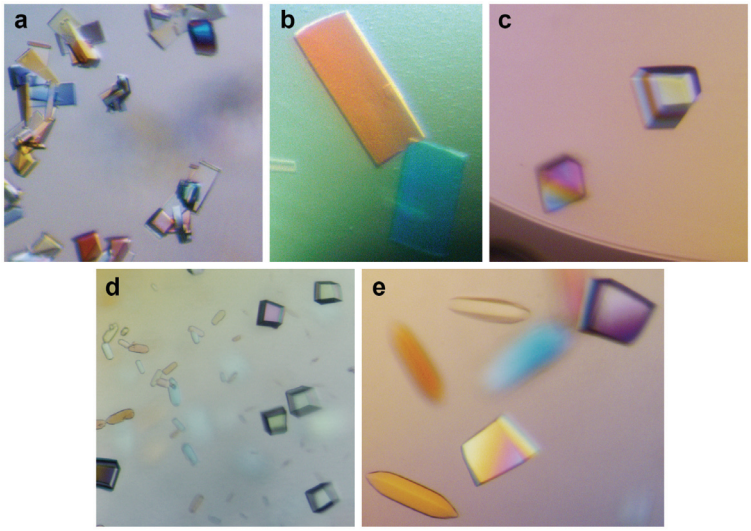

Supplementary Figure 2. Photomicrographs of ternary complex crystals. (**a**) The square-bipyramid and plate shaped crystals of $Runx1_{1-242}$•$Ets1_{296-441}$•TCRα obtained in an optimized growth condition. (**b**) and (**c**) The square-bipyramid and plate shaped crystals after macroseeding. (**d**) and (**e**) The deformed cube and rod shaped crystals of $Runx1_{48-214}$•$Ets1_{296-441}$•TCRα obtained in an optimized growth condition.

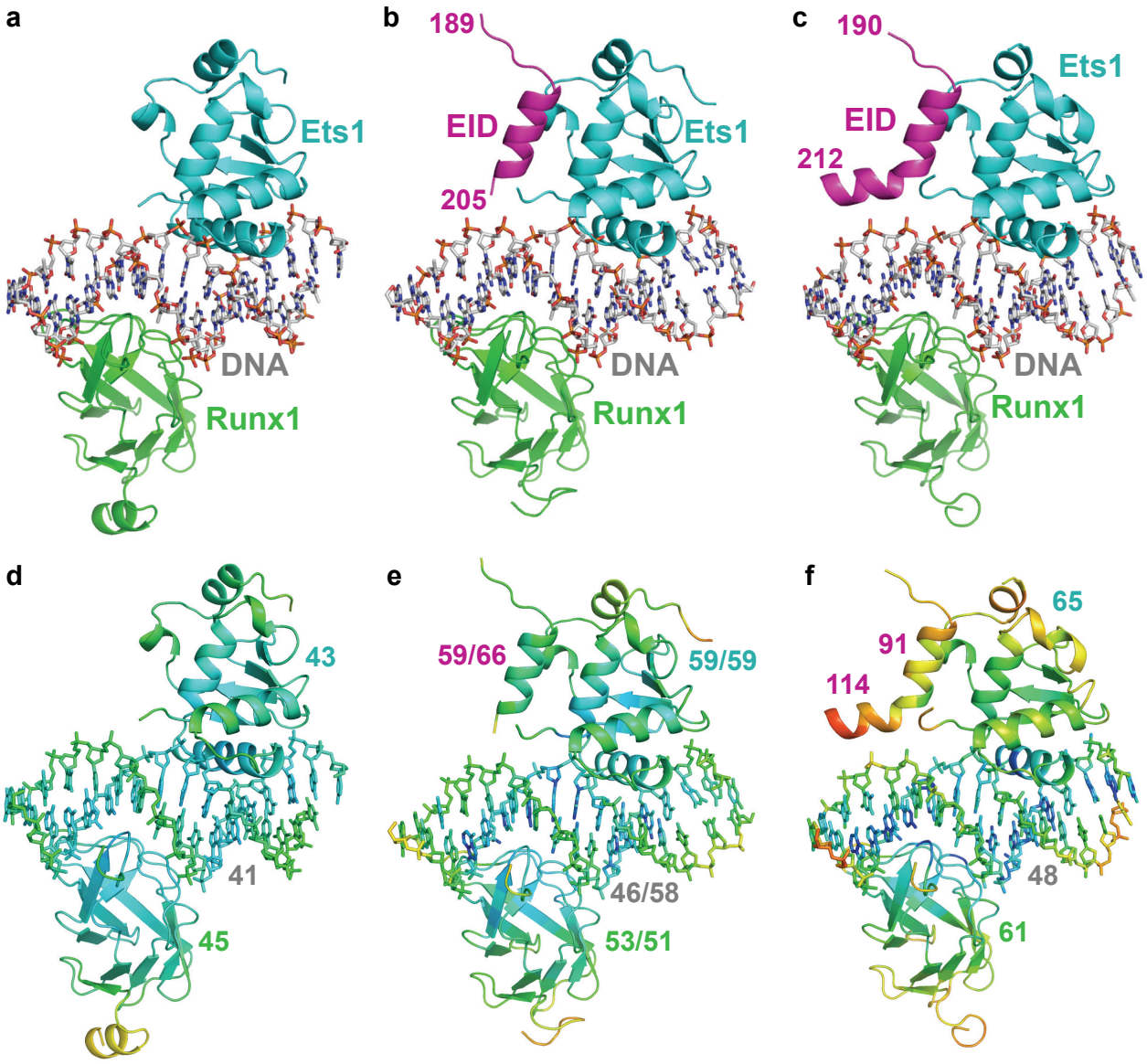

Supplementary Figure 3. Side-by-side comparison of Runx1•Ets1•TCRα ternary complexes from three different crystal structures. Overall folding of the complex from the structures of (**a**) plate shaped crystal of $Runx1_{1-242}$•$Ets1_{296-441}$•TCRα, (**b**) deformed cube shaped crystal of $Runx1_{48-214}$•$Ets1_{296-441}$•TCRα, and (**c**) square-bipyramid shaped crystal of $Runx1_{1-242}$•$Ets1_{296-441}$•TCRα. Runx1, Ets1 and EID are displayed in cartoons and DNA is displayed in sticks. Starting and ending residue numbers are indicated for the folded portions of Runx1 EID. The root-mean-square deviations (rmsd) between the structures in (a) and (b), (a) and (c), and (b) and (c), are 1.24 Å for 223 C_α atoms, 1.27 Å for 212 C_α atoms, and 0.35 Å for 236 C_α atoms, respectively. Only one of two protomers in deformed cube shaped crystal is shown in panel (b). The rmsd between the protomers is 0.17Å for 244 C_α atoms. Distribution of B-factors in the complexes from (**d**) plate shaped crystal of $Runx1_{1-242}$•$Ets1_{296-441}$•TCRα, (**e**) deformed cube shaped crystal of $Runx1_{48-214}$•$Ets1_{296-441}$•TCRα, and (**f**) square-bipyramid shaped crystal of $Runx1_{1-242}$•$Ets1_{296-441}$•TCR. The spectrum is changing from blue (the lowest B-factors) to green, yellow and red (the highest B-factor). Average B-values in $Å^2$ are shown for each subunit and separately for EID helices.

Supplementary Figure 4. Quality of Runx1 EID electron density maps. A stereoview of $2F_o$-F_c Fourier maps for the first and second ternary complex protomers in crystal structure of $Runx1_{48-214}$•$Ets1_{296-441}$•TCRα (**a** and **b**), and in crystal structure of $Runx1_{1-242}$•$Ets1_{296-441}$•TCRα (square-bipyramid form). (**c**) The maps are drawn at density level of 1σ and show the density of EID residues and surrounding residues from Ets1 and DNA.

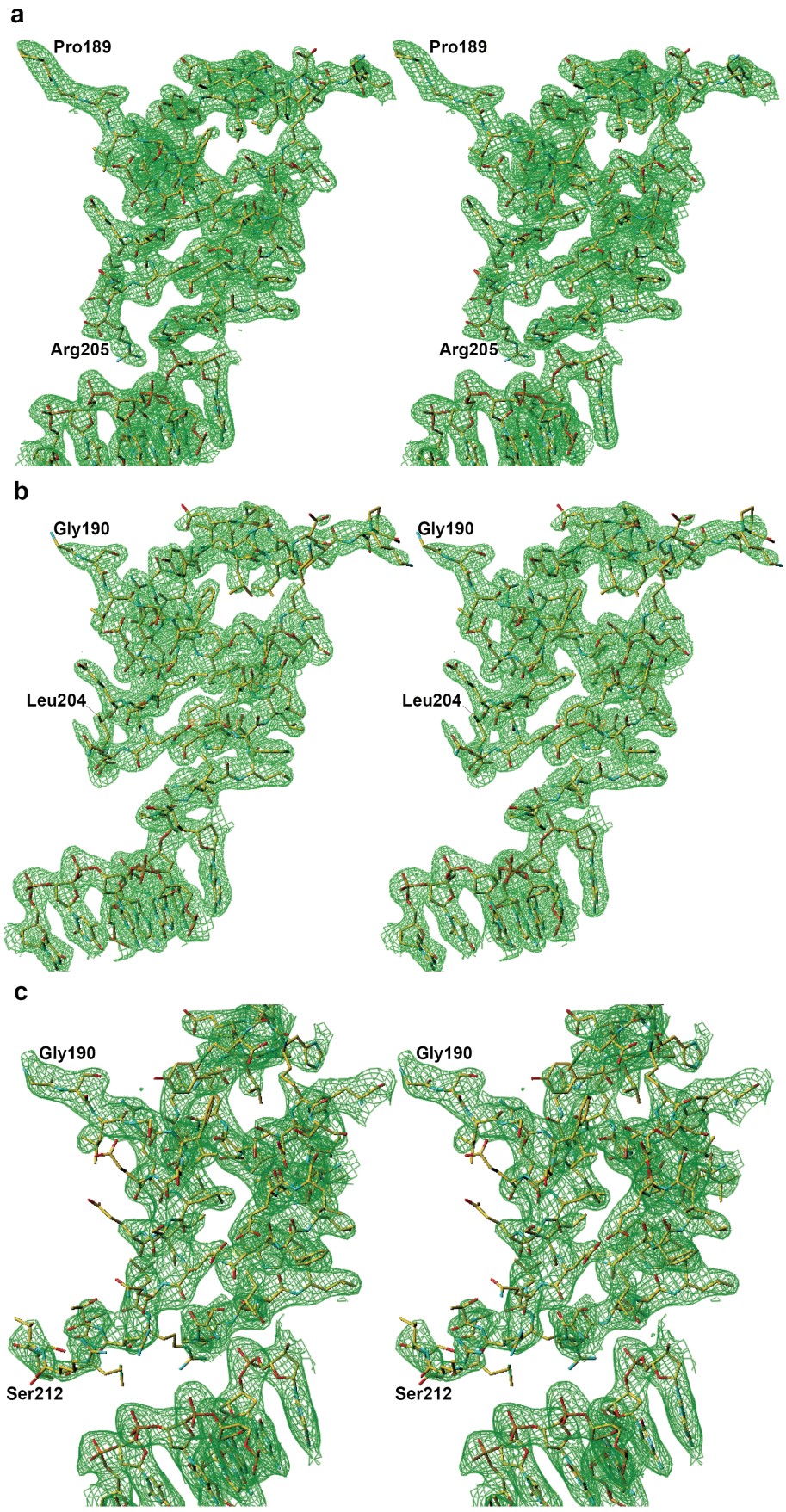

Supplementary Figure 5. Crystal packing effects to the folding of Ets1 and EID. (**a**) Location of Ets1 C-terminal residues (1gvj) shown in palecyan after superimposition with Ets1 in square-bipyramid crystal. The comparison indicates that Pro68′ and Asn69′ from RD of symmetry-related molecule (RD′) are in conflict with Ets1 C-terminal residues, resulting in their disorder. (**b**) Comparison of square-bipyramid (ED is in cyan and EID is in magenta) and plate shaped crystal (ED in light grey and RD′ is in dark grey) structures after superimposition of their EDs. The RD′ in plate crystal shifts the C-terminal residues of ED to a conformation that is not favorable for the docking of EID. (**c**) Comparison of square-bipyramid (EID is in magenta and RD′ is in green) and deformed cube crystal (EID and RD′ are in dark grey) structures after superimposition of their EIDs. The RD′ in a deformed cube crystal is shifted relative to corresponding RD′ in a square-bipyramid crystal towards the α2 helix of EID. This prevents proper folding of α2 helix of EID in a deformed cube crystal.

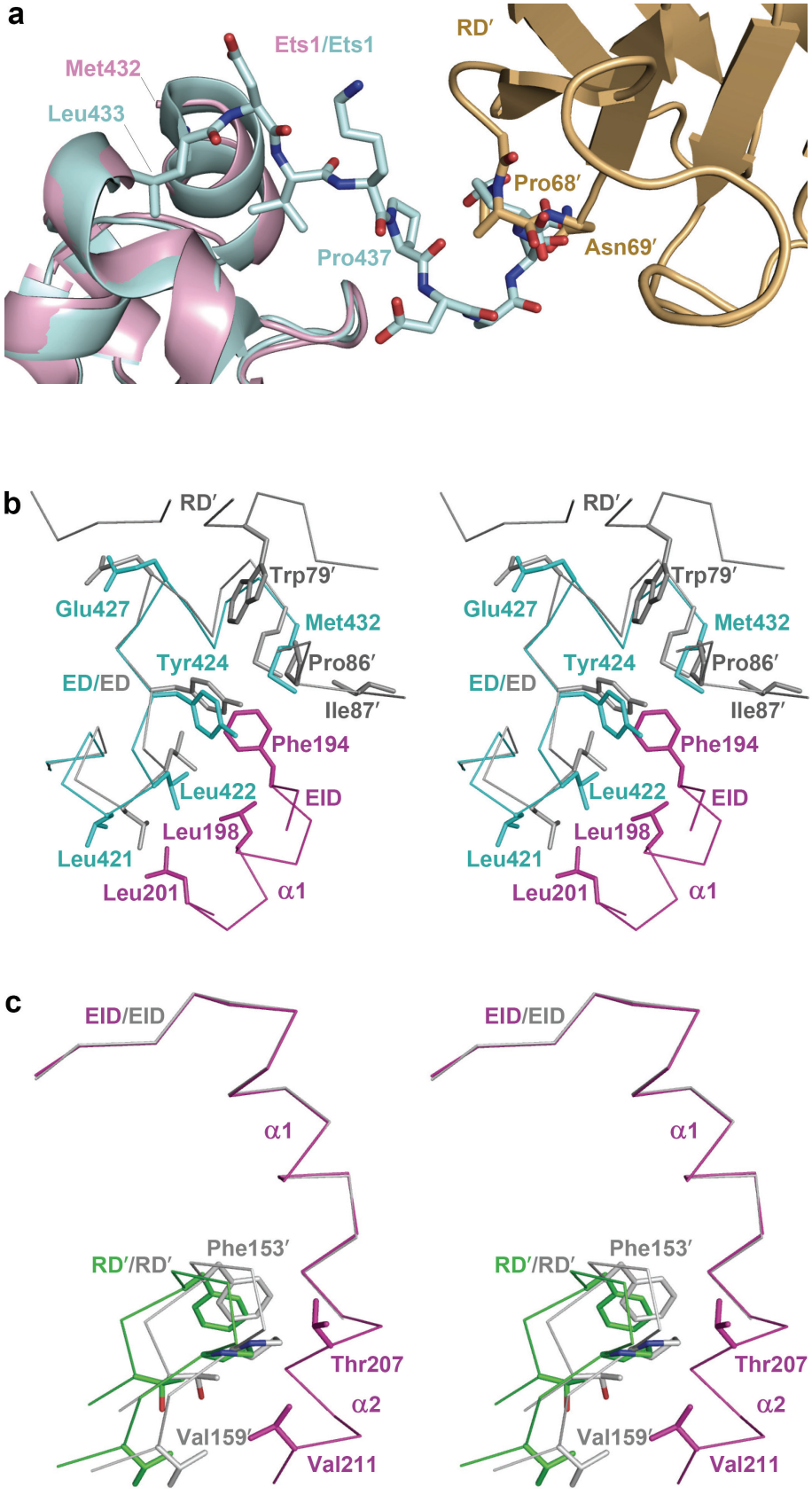

Supplementary Figure 6. Potential hydrogen bonds of Runx1 Arg 205 side chain with TCRα DNA. The donor to acceptor distances are provided in Angstroms.

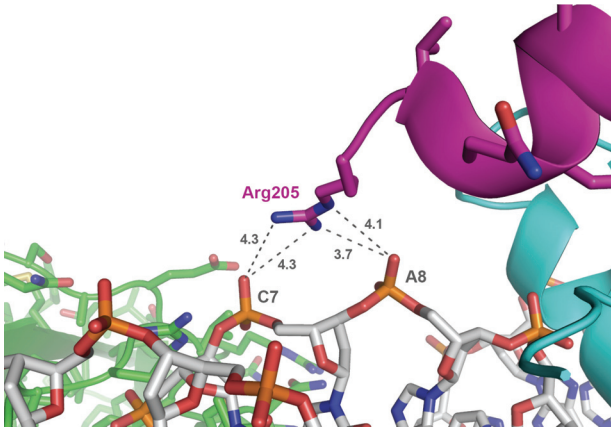

Supplementary Figure 7. Comparison of Ets1 and Runx1 DNA-binding domains in Runx1$_{1-242}$•Ets1$_{296-441}$•TCRα complex with reported structures. (**a**) Comparison with RD (brown) in structure of Runx$_{160-182}$•DNA (PDB code 1hjc). The rmsd between the RD′s is 0.35 Å for 117 C_α atoms. (**b**) Comparison with Ets domain (blue) in structure of (Ets1)$_2$•2DNA (PDB code 3ri4). The rmsd between the ED′s is 0.48 Å for 100 C_α atoms.

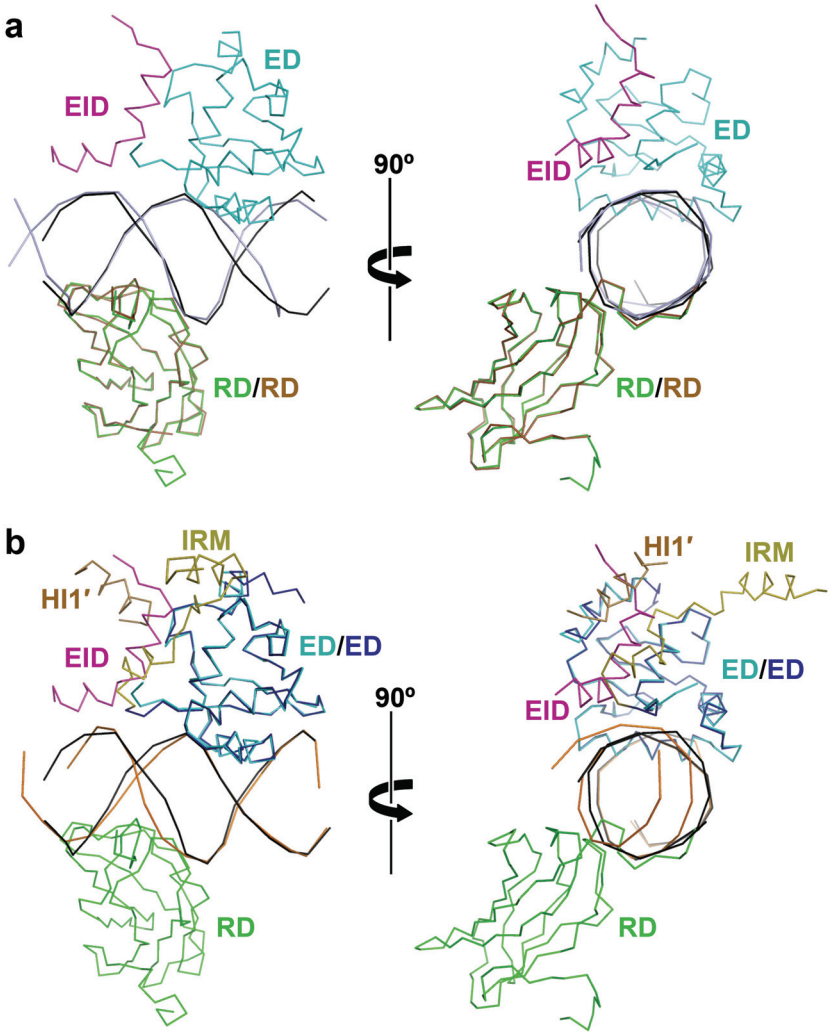

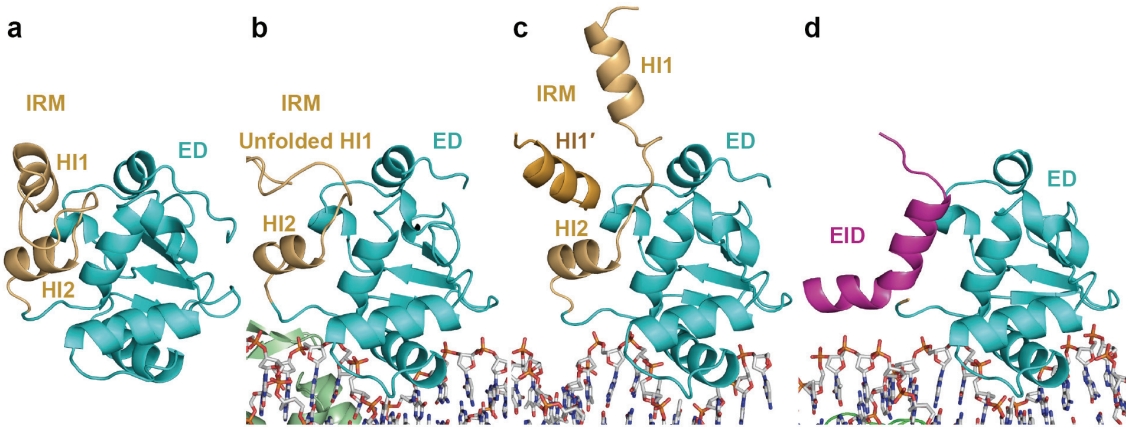

Supplementary Figure 8. Comparison of DNA-free and DNA-bound Ets1 structures highlighting different pattern for Ets1 IRM folding. (**a**) NMR structure of free Ets1 (PDB code 1R36). Both inhibitory helices HI1 and HI2 of IRM are folded in this structure. (**b**) Crystal structure of Ets1•Pax5•DNA ternary complex (1MDM) showing unfolding of HI1. HI2 remains folded in this complex. (**c**) Crystal structure of Ets1 dimer bound to *stromelysin-1* promoter DNA (3MFK). In this structure both HI1 and HI2 are folded. Symmetry related HI1 interacting with H4 is shown as HI1′. (**d**) Crystal structure of Runx1$_{1\text{-}242}$•Ets1$_{296\text{-}441}$•TCRα ternary complex. Entire IRM of Ets1 is disordered and replaced by EID of Runx1.

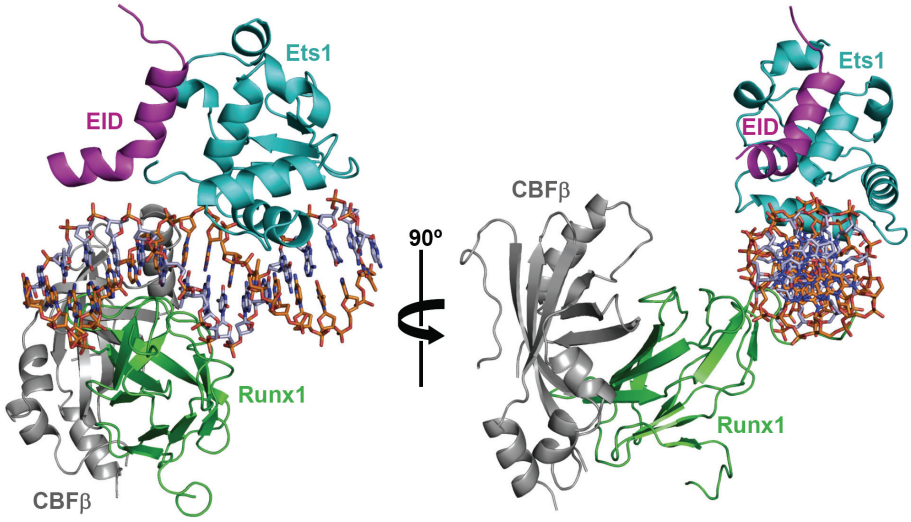

Supplementary Figure 9. Model of Runx1$_{1\text{-}242}$•Ets1$_{296\text{-}441}$•CBFβ$_{1\text{-}141}$•TCRα quaternary complex. Modeling of CBFβ$_{1\text{-}141}$ was performed by rigid-body fitting of Runx1 subunit structure from Runx1•CBFβ•C/EBPβ•DNA complex (PDB access code 1IO4) into the Runx1 subunit structure from Runx1$_{1\text{-}242}$•Ets1$_{296\text{-}441}$•TCRα complex. The model confirms the absence of CBFβ$_{1\text{-}141}$ physical intervention with EID•Ets1 interaction.